JOURNAL OF Materials CHEMISTRY

# Oxidation behavior of $Ti_3AlC_2$ powders in flowing air

**X. H. Wang and Y. C. Zhou***

*High-performance Ceramic Division, Shenyang National Laboratory for Materials Science, Institute of Metal Research, Chinese Academy of Sciences, 72 Wenhua Road, Shenyang 110016, P. R. China. E-mail: yczhou@imr.ac.cn; Fax: +86-24-23891320; Tel: +86-24-23843531 ext. 55180*

***Received 15th April 2002, Accepted 11th June 2002***
***First published as an Advance Article on the web 2nd August 2002***

The oxidation behavior of $Ti_3AlC_2$ powders has been investigated in air by means of simultaneous TGA-DSC, XRD, Raman spectra, SEM, EDS and BET specific surface measurement to understand the intrinsic oxidation behavior of this newly developed ternary compound. The starting and complete oxidation temperatures determined by simultaneous TGA-DSC were 400 and 1120 °C, respectively. These temperatures are higher than those for TiC, suggesting that $Ti_3AlC_2$ is more oxidation resistant than TiC. An anomalous oxidation temperature range of 550–650 °C in which the final mass gains due to the isothermal oxidation of $Ti_3AlC_2$ powders at 550, 600 and 650 °C for 2 h are significantly greater than that at a higher temperature of 700 °C, was observed. This anomalous oxidation behavior suggests that direct reaction dominated with high oxidation kinetics in this temperature range, which was confirmed by SEM morphology observation and BET specific surface area measurement. The oxidation of $Ti_3AlC_2$ powders at temperatures below 700 °C resulted in two modifications of $TiO_2$ (anatase and rutile). At temperatures above 800 °C the oxidation products consisted of rutile $TiO_2$ and $\alpha$-$Al_2O_3$.

## 1 Introduction

$Ti_3AlC_2$ is a new member of a family referred to as structurally related layered ternary ceramics that have attracted ever-growing attention due to their unusual combination of properties.[1–12] These layered ternaries have a common formula, $T_{n+1}AX_n$ ($n = 1$–3), where T is an early transition metal, A is an A-group element (mostly IIIA and IVA), and X is either C and/or N. $Ti_3AlC_2$ was first identified in 1994 by Pietzka and Schuster[13] while investigating the Ti-Al-C ternary phase diagram, and found to be isotypic with the well-known compound $Ti_3SiC_2$.[14] The electronic structure and bonding properties of $Ti_3AlC_2$[15] determined by means of an *ab initio* pseudopotential method based on density functional theory, has indicated that the bonding in $Ti_3AlC_2$ is metallic–covalent–ionic in nature. The coexistence of three kinds of bonds enables $Ti_3AlC_2$ to exhibit properties of both ceramics and metals. This is consistent with investigations[16,17] into the mechanical, electrical properties of bulk $Ti_3AlC_2$ fabricated by two available methods, *i.e.* a hot isostatic pressing method[16] and a solid–liquid reaction synthesis with simultaneous densification process.[17] In the fabrication method proposed by Tzenov and Barsoum,[16] the disadvantages of a long synthesis time, high pressure and complex procedure are obvious. Moreover, the final materials contained an $Al_2O_3$ impurity as in the initial materials $Al_4C_3$ is hygroscopic.[16] However, the fabrication process[17] developed by the present authors has the advantages of short synthesis time, low pressure, a simple procedure and a high purity of the final product over the former.

In comparison with the well-known engineering ceramics such as SiC, $Si_3N_4$ and $Al_2O_3$, the salient characteristics of $Ti_3AlC_2$ are that it has low hardness and shear strength, therefore it can be easily machined by conventional machining method using high-speed steel tools. In addition to the good machinability, $Ti_3AlC_2$ has good thermal shock resistance and high electrical conductivity.[16,17] Our primary investigation[18] on the high-temperature oxidation behavior of bulk $Ti_3AlC_2$ at temperatures from 1000 to 1400 °C in air has demonstrated that $Ti_3AlC_2$ had good oxidation resistance, and the oxidation generally obeyed a parabolic rate law with parabolic rate constants increasing from $4.1 \times 10^{-11}$ $kg^2\ m^{-4}\ s^{-1}$ at 1000 °C to $1.7 \times 10^{-8}$ $kg^2\ m^{-4}\ s^{-1}$ at 1400 °C. The good oxidation resistance resulted from the formation of continuous $Al_2O_3$ layers on the surface of the $Ti_3AlC_2$ substrates. Furthermore, owing to the lightweight,[13] high strength,[16,17] high modulus,[19] and high electrical conductivity,[16,17] $Ti_3AlC_2$ in powder form is also a good composite reinforcement for metals such as copper and aluminium. As far as is known, published reports on the properties of $Ti_3AlC_2$ in powder form are unavailable. Therefore, it is important and interesting to investigate the properties of $Ti_3AlC_2$ in powder form. In the present paper, we reported the oxidation behavior of $Ti_3AlC_2$ powders at temperatures from 500 to 1200 °C in air.

## 2 Experimental

The $Ti_3AlC_2$ powders used in this work were obtained by a pressureless sintering procedure that is similar to the solid–liquid reaction synthesis and simultaneous *in-situ* hot pressing process[17] in the fabrication of bulk sample. This fabrication process exhibits merits that include simultaneous synthesis and densification, low pressure and short synthesis time owing to thae fact that it takes advantages of the solid–liquid reactions during the synthesis process. The difference between these two procedures is that no pressure was applied in the former. Although no pressure was applied during the synthesis process, the density of the sample prepared with the pressureless sintering procedure still reached about 50% of the theoretical density owing to solid–liquid reactions taking place during the synthesis process, and therefore can not be easily ground into powders. As a result, the $Ti_3AlC_2$ powders used in this study were obtained by drilling the sintered sample with high-speed steel drill.

Simultaneous thermal gravimetric analysis (TGA)-differential scanning calorimetry (DSC) experiments on $Ti_3AlC_2$ powders were performed in a Setsys 16/18 thermal analyzer (SETARAM, France) by heating the powder samples from

ambient temperature to 1500 °C at a rate of 10 K $min^{-1}$ in a flowing air atmosphere. $Al_2O_3$ crucibles were used in this study. Previous works have demonstrated that the structures and properties of ternary $Ti_3AlC_2$ and binary TiC are strongly related. The structure of $Ti_3AlC_2$ could be considered as a layer of Al atoms intercalated into the (111) twin boundary of TiC.[20,21] To understand the role of the Al atoms in the oxidation resistance of $Ti_3AlC_2$, TiC powders were also subjected to simultaneous TGA-DSC experiments under the same experimental conditions. Isothermal oxidation examinations were carried out in the temperature range 500–1200 °C for 2 h in flowing air. By doing the isothermal examinations, the specimens were protected in argon before reaching the required temperature; air was introduced into the furnace by a computer-controlled switch from argon to air once the required temperature was reached. Phase identification of the samples after oxidation was performed using X-ray diffraction (XRD) and Raman spectra. XRD examinations were carried out in a D/max rA X-ray diffractometer (Rigaku, Japan), and the Raman spectra were recorded at room temperature in a LabRam HR 800 Raman spectrometer using a He–Ne laser with wavelength of 632.8 nm as the excitation source. Morphological observation was conducted on a 6301F field emission scanning electron microscope (JEOL, Japan) equipped with an energy dispersive spectroscopy (EDS) system. The BET specific surface area was determined by calculating the volume of adsorbed nitrogen at 77 K. The BET specific surface area measurements were conducted in an ASAP 2010 volumetric analyzer.

## 3 Results and discussion

### 3.1 Simultaneous TGA-DSC

It is known that titanium carbide (TiC) exhibits a rather limited oxidation resistance. A mass increase was observed when TiC was treated under an oxygen pressure between 4 and 16 kPa at a temperature as low as 350 °C.[22] Titanium oxycarbides and suboxides were assumed to be formed at the initial stage of the oxidation process. Non-protecting anatase $TiO_2$ layers were detected in the oxidation conducted up to 700 °C. As rutile $TiO_2$ layers were formed between 700 and 900 °C, a detrimental further oxidation was observed as a result of cracks occurring in the oxide layers when they became thick.[23] Owing to the presence of aluminium in the ternary phase $Ti_3AlC_2$, the oxidation behavior of this compound should be somewhat different from that of TiC and the role played by aluminium should be investigated.

Simultaneous TGA-DTG-DSC curves for $Ti_3AlC_2$ are presented in Fig. 1. It can be seen that the shape of DSC is consistent with that of DTG. This indicates that the change in mass gain rate (DTG signal) resulted from the corresponding

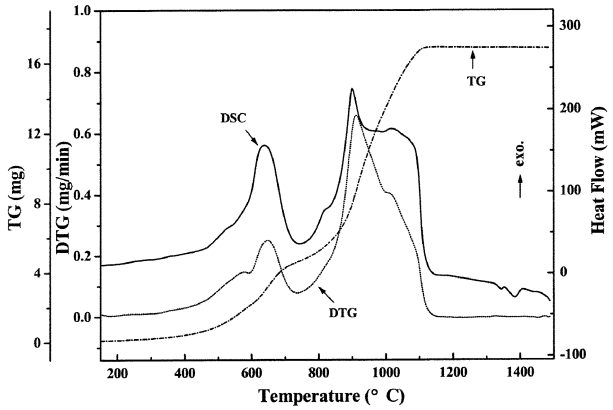


**Fig. 1** TGA-DTG-DSC curves recorded during heating of $Ti_3AlC_2$ powders up to 1500 °C at a rate of 10 K $min^{-1}$ in flowing air.

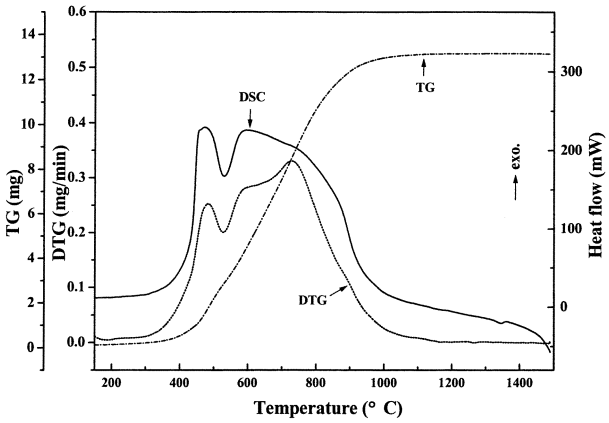


**Fig. 2** TGA-DTG-DSC curves recorded during heating of TiC powders up to 1500 °C at a rate of 10 K $min^{-1}$ in flowing air.

reactions associated with exothermic effect (DSC signal). The DTG and DSC curves were divided into two parts by an apparent gap between 650 and 850 °C. An obvious mass increase occurred near 400 °C and the mass increase terminated at 1120 °C, suggesting that the starting oxidation and complete oxidation temperatures of $Ti_3AlC_2$ were 400 and 1120 °C, respectively. To understand the difference in oxidation resistance between $Ti_3AlC_2$ and TiC, TiC powders were also subjected to simultaneous TGA-DSC examination under the same experimental condition. Fig. 2 shows the simultaneous TGA-DTG-DSC curves for TiC. Similar to the oxidation of $Ti_3AlC_2$, the shape of DSC curve is also in good agreement with that of DTG curve. However, no slow increase of mass gain in the TGA curve at 650–850 °C was observed. Moreover, the obvious mass increase occurred near 350 °C, which is in agreement with a previous report,[22] and the mass increase terminated at 1000 °C. The two typical temperatures for TiC are lower than those for $Ti_3AlC_2$, indicating that $Ti_3AlC_2$ had better oxidation resistance than TiC because of the intercalation of Al into TiC to form ternary $Ti_3AlC_2$.

### 3.2 Isothermal oxidation at 500–1200 °C

The isothermal relative mass variations as a function of time at temperatures between 500 and 1200 °C under flowing air are shown in Fig. 3. The isotherms exhibit two steps, *i.e.*, the first, a rapid oxidation step and the second, a slow oxidation step. This first step corresponds to very rapid oxidation kinetics, the mass gain in the first hour varied from 3 to 49% depending on the oxidation temperature. The second step is a slower oxidation

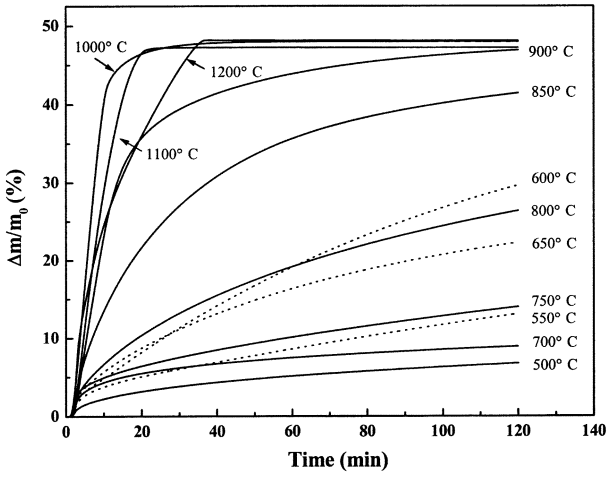


**Fig. 3** Isothermal weight changes of $Ti_3AlC_2$ powders exposed to air at 500–1200 °C as a function of time. Anomalous isotherms at 550, 600 and 650 °C are plotted as dotted lines.

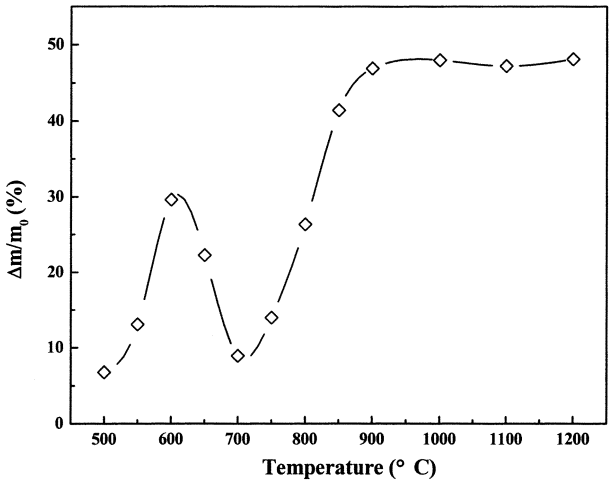


**Fig. 4** Final weight gain *versus* oxidation temperature, indicating anomalous weight gains in the temperature range 550–650 °C.

process with a mass increase of less than 10% for 2 h treatment in most cases. This two-step behavior is enhanced at temperatures higher than 1000 °C. Fig. 4 shows the temperature dependence of the ultimate mass gain in the temperature range 500–1200 °C. It should be noted that the ultimate mass gains owing to the oxidation at temperatures between 550–650 °C are larger than that at higher temperatures, *e.g.*, 700 °C. This suggests that an anomalous oxidation with high kinetics occurred near 600 °C. This anomalous oxidation will be discussed in detail below. It is also interesting to find that the slopes of the isotherms in the first oxidation step for the samples oxidized at 1100 and 1200 °C are less than that for the sample oxidized at 1000 °C, as indicated by arrows shown in Fig. 3.

To understand the oxidation behavior of $Ti_3AlC_2$ at different temperatures, the samples after a 2 h oxidation were characterized from a physico-chemical point of view; phase identification by XRD and Raman spectra, morphology by SEM, elemental analysis by EDS and specific surface measurement by the BET method at 77 K. The results are described and discussed in the following sections.

### 3.3 X-ray diffraction and Raman spectra

As described above, an anomalous oxidation occurred between 550 and 650 °C. Since the ultimate mass gains owing to the exposure to air atmosphere for 2 h at 550, 600 and 650 °C are greater than the sample oxidized at 700 °C, it is worth investigating this abnormal phenomenon. Phase identification of the samples after exposure to air for 2 h was firstly determined using XRD. Fig. 5 show the powder XRD patterns of the samples exposed at temperatures of 500, 600, 700, 800, 900 and 1200 °C. At the lowest temperature of 500 °C in this study, no other phase in crystalline form but $Ti_3AlC_2$ was detected within the resolution of the diffractometer. At 600 °C, however, oxide phases, including two modifications of $TiO_2$ (*i.e.* anatase and rutile), were identified and the intensities of the diffraction peaks for $Ti_3AlC_2$ profoundly decreased. At 700 °C, no new crystalline phase was detected but the intensities of the diffraction peaks for $Ti_3AlC_2$ significantly increased in comparison to the sample oxidized at 600 °C, indicating that $Ti_3AlC_2$ suffered further oxidation at 600 °C and consequently there remained less $Ti_3AlC_2$ in the final oxidized specimen. By analyzing the powder XRD patterns of the samples oxidized at 500, 600 and 700 °C, it is reasonable to conclude that the sample oxidized at 600 °C contained a larger amount of oxides (Fig. 5) than that oxidized at 700 °C, which is in good agreement with the Raman spectra. Fig. 6 presents the Raman spectra of the samples after oxidation at 500, 600 and 700 °C. The characteristic Raman peaks at 447 $cm^{-1}$ ($E_g$) and 610 $cm^{-1}$ ($A_{1g}$) for rutile $TiO_2$[24]

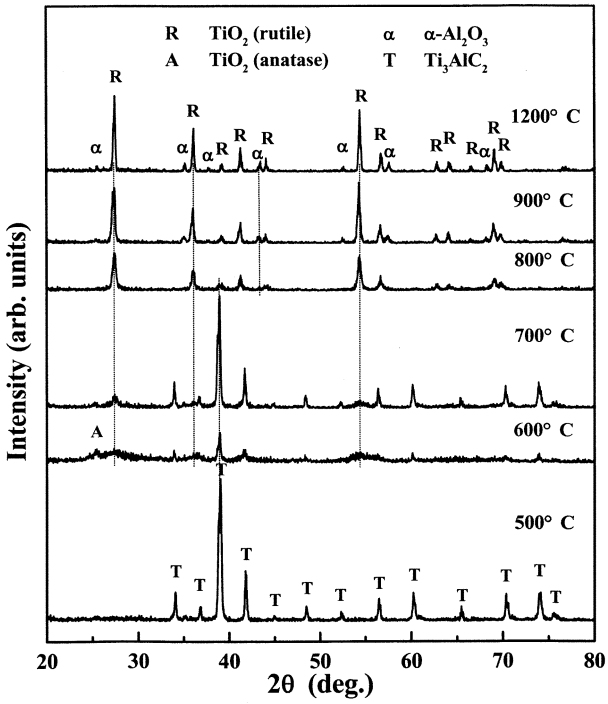


**Fig. 5** Powder XRD patterns of $Ti_3AlC_2$ powders oxidized at 500, 600, 700, 800, 900 and 1200 °C in air for 2 h.

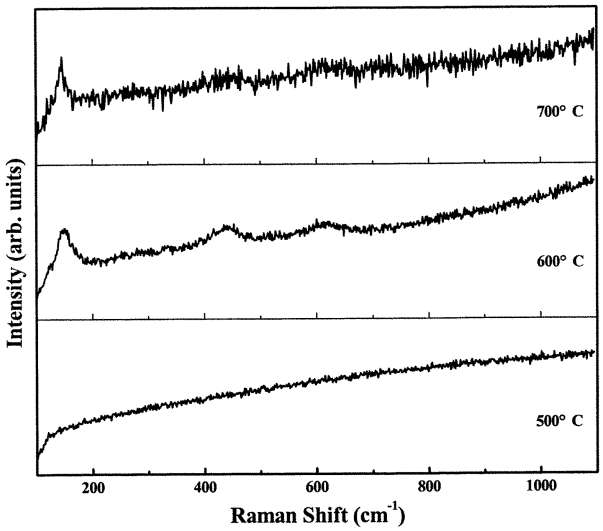


**Fig. 6** Raman spectra of samples after oxidation at 500, 600 and 700 °C.

were only obviously observed for the sample oxidized at 600 °C. It is well acknowledged that if the oxidation is diffusion controlled, the extent of oxidation should increase with the temperature. So in the present study, the anomalous oxidation of $Ti_3AlC_2$ between 550 and 650 °C obeyed another oxidation law with high kinetics rather than the diffusion controlled law. At 800 °C, rutile $TiO_2$ dominated, with a small amount of $Ti_3AlC_2$ that had been mostly oxidized, also the strongest diffraction peak at $d = 2.0482$ for $\alpha$-$Al_2O_3$ was detected. The presence of $\alpha$-$Al_2O_3$ in the sample oxidized at 800 °C was confirmed in the Raman spectrum. Fig. 7 shows the Raman spectrum of the specimen oxidized at this temperature. Two strong Raman peaks at 1355 and 1389 $cm^{-1}$ are associated with the Raman shifts of $\alpha$-$Al_2O_3$.[25] Besides $\alpha$-$Al_2O_3$, rutile $TiO_2$ was also identified by Raman shifts at 447 $cm^{-1}$ ($E_g$) and 610 $cm^{-1}$ ($A_{1g}$), which are characteristic peaks for rutile $TiO_2$[24] (see inset of Fig. 7). By increasing the temperature up to 1200 °C, no new phases were detected with only the sharpness of the diffraction peaks associated with $\alpha$-$Al_2O_3$ and rutile $TiO_2$, as

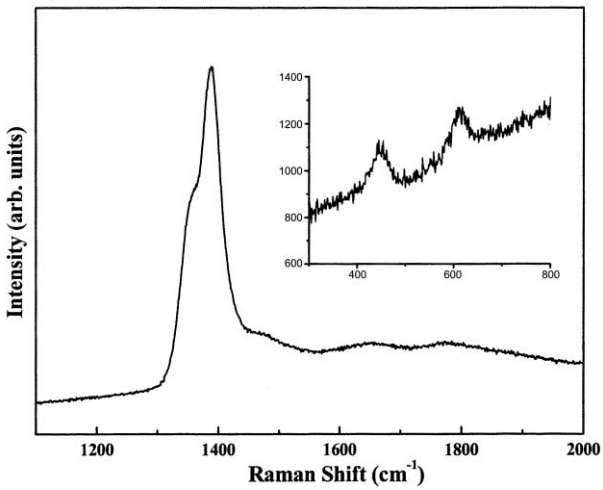


**Fig. 7** Raman spectrum of a sample after oxidation at 800 °C showing the characteristic Raman peaks for $\alpha$-$Al_2O_3$,[25] and those for rutile $TiO_2$[24] (see inset).

shown in Fig. 5. Since no new phases were formed in the temperature range 1000–1200 °C, the decrease in the slopes of the isotherms with temperature should be attributed to the formation rate of oxides on the surface of the $Ti_3AlC_2$ particles. In this case, the most possible reason for this decrease with temperature is associated with the formation rate of $Al_2O_3$ instead of rutile $TiO_2$, because $Al_2O_3$ is much more protective than $TiO_2$. With increasing temperature, protective oxides were formed more rapidly and gave the slower oxidation rate in the first steps (see Fig. 3).

### 3.4 SEM morphology and BET specific surface area

The morphologies and elemental analyses of the samples after exposure to air at various temperatures were also carried out in an SEM equipped with an EDS system. At 500 °C, the $Ti_3AlC_2$ grains with laminated morphology remain intact (not shown). By increasing the temperature to 600 °C, a number of cracks were obviously observed on the grains. Fig. 8(a) shows the SEM microstructure of the sample after exposure to air at 600 °C. Also the cracks occurred particularly along the laminations as shown in Fig. 8(b), the high-magnification microstructure of the cracked grains. Cracks were observed in the study of the oxidation of titanium carbide at 400 °C by Shimada and Kozeki.[22] They attributed the cracks to the stress developed with the anatase layer and resulting from the volume expansion associated with the oxidation of TiC into anatase. Similar cracks were also reported by Racault *et al.*[26] in the oxidation of $Ti_3SiC_2$ at 650 °C in oxygen. Previous work by Zhou *et al.*[15] has demonstrated that in the layered compound $Ti_3AlC_2$, the bonding between the Ti layers parallel to the basal plane and the neighboring Al layers is weak. If the stress arises owing to the volume expansion associated with the oxidation of $Ti_3AlC_2$ into anatase, cracks will preferentially occur along the laminations between which the bonding is weak. For the sample exposed at 700 °C, the morphology is quite different from that of the samples exposed to air at 600 °C, there were almost no obvious cracks visible, as shown in Fig. 9(a). The lack of cracks in the grains enables $Ti_3AlC_2$ to have good oxidation resistance at 700 °C. The elemental analysis results of the samples oxidized at 500, 600, 700 and 800 °C using EDS are summarized in Table 1. It can be seen that for the sample oxidized at 600 °C, the oxygen content reached the highest value, in other words, the sample suffered more serious oxidation, which is consistent with the XRD results (Fig. 5) and the Raman spectra (Fig. 6). For the sample oxidized at 800 °C, each particle was homogeneously covered with a layer of very small grains, as shown in Fig. 9(b). Fig. 9(c) presents a

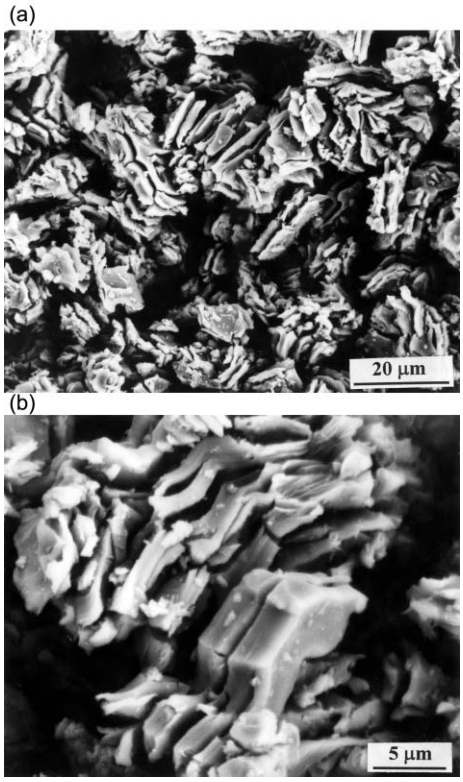


**Fig. 8** (a) SEM micrographs of specimens oxidized at 600 °C indicating that a number of cracks were present within the $Ti_3AlC_2$ grains; (b) higher magnification micrograph showing that the cracks occurred particularly along the laminations.

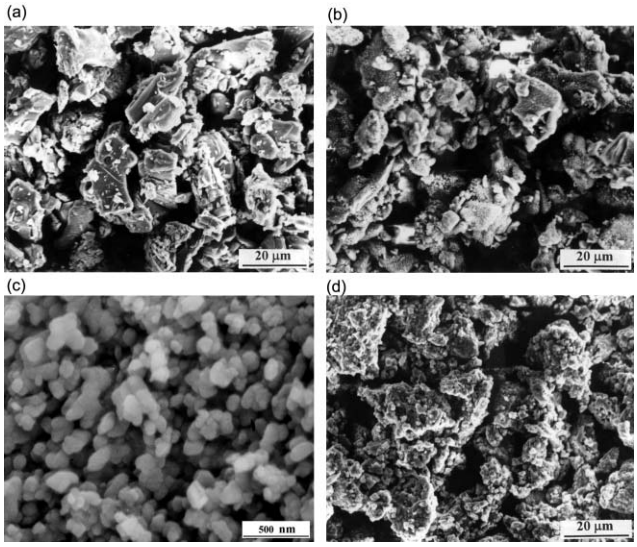


**Fig. 9** SEM microstructures of specimens oxidized at: (a) 700 °C, indicating the $Ti_3AlC_2$ grains remained intact; (b) 800 °C, showing that the particles were covered with a layer of smaller grains; (c) higher magnification micrograph of the smaller grains on the particles shown in Fig. 9(b); and (d) at 1200 °C, indicating the pores distributed on the particles containing rutile $TiO_2$ and $\alpha$-$Al_2O_3$.

**Table 1** Summary of elemental analysis using EDS for samples oxidized at temperatures of 500–800 °C

| Temperature/°C | Elemental content (at.%) | | | Al/Ti atomic ratio |
|---|---|---|---|---|
| | O | Al | Ti | |
| 500 | 58.1 | 9.7 | 32.3 | 0.30 |
| 600 | 70.0 | 8.2 | 21.8 | 0.38 |
| 700 | 61.5 | 8.4 | 30.2 | 0.28 |
| 800 | 74.6 | 10.1 | 15.3 | 0.66 |

higher magnification micrograph of the particle. It is clearly observed that uniform nano-size grains distribute on the particle. These small grains probably correspond to $Al_2O_3$. By carefully analyzing the elemental contents shown in Table 1, the Al : Ti atomic ratio of the sample oxidized at 800 °C is much higher than the remaining, which means that elemental Al distributed outward. As revealed by XRD result (Fig. 5) and Raman spectrum (Fig. 7), $Al_2O_3$ has been identified in the sample oxidized at 800 °C. Therefore, it is plausible to attribute the small grains to $Al_2O_3$. Formation of stable $Al_2O_3$ on the surface of $Ti_3AlC_2$ is important at this temperature, and would enable bulk $Ti_3AlC_2$ to have good oxidation resistance. To confirm the formation of a protective $Al_2O_3$ layer on the $Ti_3AlC_2$ needs further work, which is in progress in the present authors' laboratory. Fig. 9(d) shows an SEM micrograph of a sample oxidized at 1200 °C, it can be seen that the particles are porous with a number of pores distributed uniformly.

The formation of cracks during the oxidation process makes the oxides non-protecting and will consequently increase the specific surface area. In an attempt to confirm this, and to evaluate the extent of the increase in the specific surface area owing to the formation of cracks for the sample exposed to air at 600 °C, the other two typical samples oxidized at 500 and 700 °C, together with the sample oxidized at 600 °C, were subjected to BET specific surface area measurements. The BET specific surface area of the sample oxidized at 600 °C reached 55.7 $m^2\ g^{-1}$, whereas those exposed to air at 500 and 700 °C were only 2.70 and 4.48 $m^2\ g^{-1}$, respectively. At this point, it is reasonable to conclude that for the sample exposed at 600 °C the limited oxidation resistance originates from the continuous increase of fresh surface due to the formation of cracks during oxidation.

On the basis of the above investigations, the oxidation behavior of $Ti_3AlC_2$ powders can be deduced according to the three temperature ranges. In the first temperature range, *i.e.* 550–700 °C, the oxidation process yields two modifications of $TiO_2$. The $TiO_2$ film formed as a result of the reaction with oxygen protects only at 700 °C, and consequently resulted in less weight gain (Fig. 3). For the remaining temperatures, no protective films were established because of the formation of cracks.

In the second temperature range, *i.e.* 700–1000 °C, the oxidation showed a diffusion-controlled process, and was profoundly enhanced with increasing temperature.

In the third temperature range, *i.e.* 1000–1200 °C, the oxidation process was rapid with high oxidation kinetics, and was completely finished within 35 min.

## 4 Conclusion

The oxidation behavior of $Ti_3AlC_2$ powders has been investigated in air by means of simultaneous TGA-DSC, XRD, Raman spectra, SEM, EDS and BET specific surface measurement to understand the intrinsic oxidation behavior of this newly developed ternary compound. The oxidation starts at 400 °C, which is slightly higher than that for TiC, suggesting that Al plays a positive role in promoting the oxidation resistance of $Ti_3AlC_2$. An anomalous oxidation phenomenon in the temperature range 550–650 °C, was observed. The formation of cracks led to high oxidation kinetics in this temperature range and this accounts for the anomalous oxidation. This suggests that this material should avoid being directly exposed to air in the temperature range 550–650 °C. The oxidation of $Ti_3AlC_2$ powders at temperatures below 700 °C gave two modifications of $TiO_2$ (anatase and rutile). At temperatures above 800 °C the oxidation products consisted of rutile $TiO_2$ and $\alpha$-$Al_2O_3$.

## Acknowledgements

This work was financially supported by the National Outstanding Young Scientist Foundation for Y.C. Zhou under Grant No.59925208, the National Science Foundation of China (NSFC) under Grant No. 50072034, '863' program and the IMR Innovative Research Foundation.

## References

1 S. Arunajatesan and A. H. Carim, *J. Am. Ceram. Soc.*, 1995, **78**, 667.
2 M. W. Barsoum and T. El-Raghy, *J. Am. Ceram. Soc.*, 1996, **79**, 1953.
3 M. W. Barsoum, T. El-Raghy and L. Ogbuji, *J. Electrochem. Soc.*, 1997, **144**, 2508.
4 Y. C. Zhou and Z. M. Sun, *Mater. Res. Innovations*, 1999, **3**, 171.
5 M. W. Barsoum, M. Ali and T. El-Raghy, *Metall. Mater. Trans. A*, 2000, **31**, 1857.
6 A. T. Procopio, M. W. Barsoum and T. El-Raghy, *Metall. Mater. Trans. A*, 2000, **31**, 333.
7 Y. C. Zhou and X. H. Wang, *Mater. Res. Innovations*, 2001, **5**, 87.
8 X. H. Wang and Y. C. Zhou, *Z. Metallkd.*, 2002, **93**, 66.
9 A. Crossley, E. H. Kisi, J. W. B. Summers and S. Myhra, *J. Phys. D: Appl. Phys.*, 1999, **32**, 632.
10 H.-I. Yoo, M. W. Barsoum and T. El-Raghy, *Nature*, 2000, **407**, 581.
11 Z. M. Sun, Y. C. Zhou and M. S. Li, *Corros. Sci.*, 2001, **43**, 1095.
12 X. H. Wang and Y. C. Zhou, *Acta Mater.*, 2002, **50**, 3143.
13 M. A. Pietzka and J. C. Schuster, *J. Phase Equilib.*, 1994, **15**, 392.
14 W. Jeitschko and H. Nowotny, *Monatsh. Chem.*, 1967, **98**, 329.
15 Y. C. Zhou, X. H. Wang, Z. M. Sun and S. Q. Chen, *J. Mater. Chem.*, 2001, **11**, 2335.
16 N. V. Tzenov and M. W. Barsoum, *J. Am. Ceram. Soc.*, 2000, **83**, 825.
17 X. H. Wang and Y. C. Zhou, *J. Mater. Chem.*, 2002, **12**, 455.
18 X. H. Wang and Y. C. Zhou, *Corros. Sci.*, submitted.
19 M. W. Barsoum and T. El-Raghy, *J. Appl. Phys.*, 2000, **87**, 1701.
20 Y. C. Zhou, Z. M. Sun and B. H. Yu, *Z. Metallkd.*, 2000, **91**, 937.
21 M. W. Barsoum, *Scr. Mater.*, 2000, **43**, 285.
22 S. Shimada and M. Kozeki, *J. Mater. Sci.*, 1992, **27**, 1869.
23 Y. A. Lavrenko, L. A. Glebov, A. P. Pomitkin, V. G. Chuprina and T. G. Protsenko, *Oxid. Met.*, 1975, **9**, 171.
24 S. P. S. Porto, P. A. Fleury and T. C. Damen, *Phys. Rev.*, 1967, **154**, 522.
25 A. Aminzadeh, *Appl. Spectrosc.*, 1997, **51**, 817.
26 C. Racault, F. Langlais and R. Naslain, *J. Mater. Sci.*, 1994, **29**, 3384.